

Accepted Manuscript

## *Geological Society, London, Special Publications*

### A multidisciplinary approach for the quantitative provenance analysis of siltstone. Mesozoic Mandawa Basin, southeastern Tanzania)

Luca Caracciolo, Sergio Andò, Pieter Vermeesch, Eduardo Garzanti, Ross McCabe, Marta Barbarano, Chiara Paleari, Martin Rittner & Timothy Pearce

DOI: <https://doi.org/10.1144/SP484-2018-136>

Received 18 July 2018

Revised 21 February 2019

Accepted 26 February 2019

© 2019 The Author(s). Published by The Geological Society of London. All rights reserved. For permissions: <http://www.geolsoc.org.uk/permissions>. Publishing disclaimer: [www.geolsoc.org.uk/pub\\_ethics](http://www.geolsoc.org.uk/pub_ethics)

To cite this article, please follow the guidance at <https://www.geolsoc.org.uk/onlinefirst#how-to-cite>

#### **Manuscript version: Accepted Manuscript**

This is a PDF of an unedited manuscript that has been accepted for publication. The manuscript will undergo copyediting, typesetting and correction before it is published in its final form. Please note that during the production process errors may be discovered which could affect the content, and all legal disclaimers that apply to the book series pertain.

Although reasonable efforts have been made to obtain all necessary permissions from third parties to include their copyrighted content within this article, their full citation and copyright line may not be present in this Accepted Manuscript version. Before using any content from this article, please refer to the Version of Record once published for full citation and copyright details, as permissions may be required.

## **A multidisciplinary approach for the quantitative provenance analysis of siltstone. Mesozoic Mandawa Basin, southeastern Tanzania)**

**Caracciolo, L.<sup>1,2</sup>, Andó, S.<sup>3</sup>, Vermeesch, P.<sup>4</sup>, Garzanti, E.<sup>3</sup> McCabe, R.<sup>2</sup>, Barbarano, M.<sup>2</sup>, Paleari<sup>3</sup>, C., Rittner, M.<sup>5</sup>, and Pearce, T.<sup>2</sup>**

1. Friedrich-Alexander Erlangen University (FAU) Erlangen-Nuremberg, GeoZentrum Nordbayern, Schlossgarten 5, 91054, Erlangen, Germany
2. Chemostrat Ltd., 1 Ravenscroft Court, Buttington Enterprise Park, Welshpool, SY21 8SL, United Kingdom
3. Laboratory for Provenance Studies, Department of Earth and Environmental Sciences, University of Milano-Bicocca, 20126 Milano, Italy
4. London Geochronology Centre, Department of Earth Sciences, University College London, London WC1E 6BT, U.K.
5. TOFWERK AG, Uttigenstr. 22, 3600 Thun, Switzerland.

### **ABSTRACT**

This paper shows how heavy minerals and single-grain varietal studies can be conducted on silt (representing ~ 50% of world's sediments) sediments to obtain quantitative data as efficiently as for sand-sized sediments. The analytical workflows include heavy mineral separation using a wide grain-size window (15-355  $\mu$ ) analysed through integrated optical analysis, RAMAN spectroscopy, QEMSCAN microscopy, U-Pb dating of detrital zircon. Upper Jurassic-Cretaceous silt-sized sediments from the Mandawa basin of central-southern Tanzania have been selected for the scope of this research. Raman-aided heavy mineral analysis reveals garnet and apatite to be the most common minerals together with durable zircon, tourmaline and subordinate rutile. Accessory but diagnostic phases are titanite, staurolite, epidote, and monazite. Etch pits on garnet and cockscomb features on staurolite document the significant effect of diagenesis on the pristine heavy mineral assemblage. Multivariate statistical analysis highlights a close association among durable minerals (zircon, tourmaline and rutile, ZTR) while garnet and apatite plot alone reflecting independence between the three group of variables with garnet increasing in Jurassic samples. Raman data for garnet end-member analysis document different associations between Jurassic (richer in A, Bi and Bii types) and Cretaceous (dominant A, Ci and Cii types) samples. U-Pb dating of detrital zircon and their statistical integration with the above mentioned datasets provide further insights on changes in provenance and/or drainage systems. Metamorphic rocks of the early and late Pan-African orogeny terranes of the

Mozambique belt and those of the Irumide Belt acted as main source of sediment during the Jurassic. Cretaceous sediments record a broadening of the drainage system reaching as far as the Usagran-Ubendian Belt and the Tanzanian Archean Craton.

## Introduction

Provenance studies traditionally focus on the sand fraction and include a number of techniques as for instance optical and digital petrography, heavy mineral analysis, bulk-rock and single-grain geochemistry and geochronology (e.g. Gazzi, 1966, Dickinson, 1970, Valloni and Maynard, 1981, Zuffa 1985, Ingersoll, 1990, Lihou and Mange, 1996, von Eynatten and Gaupp, 1999, Garzanti et al., 2007, Andò et al. 2011, von Eynatten and Dunkl, 2012, Caracciolo et al., 2015). The provenance of other clastic sediment fractions is generally disregarded for a number of reasons. Conglomerates represent a small percentage of the sedimentary record (~1%) and generally reflect provenance from first order environments as alluvial fan, coarse grained braided and meandering rivers and more rarely deltas.

Even though the silt fraction represents ~50% of the sedimentary record, the quantitative analysis of the finer-grained portion of siliciclastic sediments is generally disregarded or limited to mineralogical (XRD) and geochemical (major, trace and REE elements) analyses (Andò et al., 2011, Caracciolo et al., 2015). However, provenance interpretations of both mineralogy and inorganic geochemistry may lead to ambiguous results, especially when evaluated in light of climate and chemical weathering (Basu et al., 2015, Garzanti et al., 2015). In fact, most of the assumptions used to constrain provenance are based on the paradigm that silt is impermeable and substantially immune to diagenetic overprint. An assumption that is easily challenged by the shale gas industry which is based on the evaluation of diagenesis, petrophysical parameters (especially porosity and permeability) and eventually reservoir quality (e.g. Armitage et al., 2010, Aplin and Macquaker, 2011, Dayal et al., 2017) . Kaolinite, illite and other clay minerals cannot be certainly attributed to weathering of the source area nor to diagenesis unless more detailed analysis are performed. Even when immobile trace elements are used for provenance (e.g. Y/Ni, Cr/V, Th/Sc – Taylor & McLennan, 1985, Nesbitt & Markovics, 1997), the resolution to which sourcing lithologies are identified is generally low and expressed in terms of mafic vs felsic, which is too low a resolution to precisely identify the specific parent rocks of the sediment. Furthermore, immobile elements (e.g. chromium, yttrium, caesium etc.) are also commonly trapped in clay minerals, either during deposition and diagenetic phases

(Frysjer and Thomas, 1960, Galen et al., 1960, Aagard et al., 1974, Maksimović et al., 1981, Syed, 1999).

The recent proliferation of analytical tools, such as Raman spectroscopy and 'quantitative evaluation of minerals by scanning electron microscopy' (QEMSCAN), allows today to obtain quantitative and semi-quantitative data to properly constrain provenance signatures recorded in the silt fraction, offering the opportunity to develop a brand-new way to tackle the analysis of fine-grained sediments. While QEMSCAN provides semi-quantitative mineralogical (volumetric) data that can be used efficiently for determining bulk-rock composition and observe rock textural parameters, Raman spectroscopy permits the quick identification of heavy minerals and is particularly useful in discriminating mineral polymorphs, such as TiO<sub>2</sub> oxides (rutile, brookite and anatase), CaCO<sub>3</sub> phases (calcite, dolomite and aragonite), metamorphic quartz and feldspar types, garnet end-members, zircon, tourmaline, amphibole and epidote types (Gasharova et al., 1997, Nasdala 2004, Bersani et al, 2009, Hoang et al., 2011, Ando et al., 2014, Skulteti et al., 2016).

Having the chance to analyse heavy minerals within the silt fraction by applying the same techniques routinely used in sandstone provenance is a paradigm shift that can permit the reconstruction of dispersal mechanisms of most fine-grained material in an unprecedented way. Sediment flux and suspended load can be better understood and efficiently linked to erosional processes (e.g. Garzanti et al., 2011) and contribute it to the reconstruction of drainage systems.

In this paper, we aim at providing a full-blown compositional approach to serve as a workflow to determine the provenance of silt material without necessarily using bulk rock geochemistry, or at least without needing to rely on uncertain variables that can't be unequivocally attributed to a specific sedimentary process (e.g. chemical weathering vs diagenetic overprint). The multidisciplinary approach includes a Raman aided heavy mineral point count (Andò et al., 2011, Garzanti et al., 2011, Andò and Garzanti, 2013) -, Raman derived garnet typing for end-member recalculation (Bersani et al., 2008), QEMSCAN analysis for automated mineral phase mapping, and detrital zircon geochronology. To investigate the level of similarity of individual cases of one/multiple dataset samples have been statistically processed using multidimensional scaling techniques in order to (i) integrate the different datasets derived from quantitative and semi-quantitative analyses, (ii) link compositional signatures to better understand drainage evolution in relation to Mesozoic stratigraphy of the Mandawa Basin, and (iii) maximise the interpretation potential. The available stratigraphic framework for the Mandawa Basin is currently under review which will

possibly result into modifications. Therefore, the results presented in the manuscript are intended to contribute to the analytical improvement used for the analysis of silt rather than solving major geological problems for the Mesozoic of southern Tanzania.

In the last decade, hydrocarbon exploration has focused on unconventional plays, producing oil and gas from shale formations and is therefore crucial to be able to apply provenance techniques not only to sand deposits but also to the finest fractions of the sediment. The analytical approach and the integration of different data sets provided in the study is particularly attractive for silty-rich unconventional plays in which reservoir quality is controlled by provenance changes through time (e.g. Montney play in western Canada, Egbobawaye, 2013, Morris et al., 2014)

### **Regional geology of Tanzania and northern Mozambique**

East African geology consists of a complex assemblage of metamorphic terranes of different composition and age and of cratons, such as the Mozambique Belt and the Tanzanian Craton (Figure 1). The latter comprises a granitoid-migmatite-gneiss terrane surrounded by schist and formed at a convergent margin prior to 2500 Ma, as indicated by zircon ages occurring at ~2660 Ma (Mansur, 2008), although ages of >3200 Ma have also been reported (e.g. Kabete, 2008). Moreover, in the north-western Tanzanian Craton, mafic rocks of ~2800-2600 Ma are reported (Cook et al., 2015, and references therein).

The Mozambique Belt (MB) constitutes part of the East African Orogen and covers much of eastern Tanzania and northern Mozambique and is predominantly composed of granulite- and amphibolite-facies rocks, and is formed of numerous crustal blocks, such as the Eastern and Western Granulites, the Cabo Delgado Nappe Complex, the Usagaran-Ubendian Belt (UUB), the Kibaran Belt (KB), and the Irumide Belt (IB, Figure 1). The Neoproterozoic–early Cambrian tectonothermal overprint is documented by metamorphic zircons, recording high-temperature and high-pressure metamorphic events at ~650-620 Ma and ~550 Ma (Kröner et al., 2003, Sommer et al., 2003, 2005). Moreover, zircon crystallisation ages of ~1150-950 Ma are recorded in parts of the MB (Kröner et al., 2003, Tenzer et al., 2006).

The UUB, located east (Usagaran Belt), south, and west (Ubendian Belt) of the Tanzanian Craton (Figure 1), is predominantly made up of granitoids and granitoid gneisses, whereas paragneisses occur less frequently (Fritz et al., 2013, and references therein). Parts of the belt underwent ultra-high pressure metamorphism, producing some eclogite-facies

rocks (Möller et al., 1995). The belt also underwent greenschist-facies regressive metamorphism with epidote ± chlorite ± titanite assemblages reported (Lawley et al., 2014, Sommer and Kröner, 2013). The UUB formed in the Palaeoproterozoic, having 2000-1800 Ma magmatic ages (Gabert and Wendt, 1974, Lenoir et al., 1994, Möller et al., 1995, Collins et al. 2004), however an early granulite-facies metamorphism dated at 2100–2025 Ma is also recorded in the Ubendian Belt (Dodson et al., 1975, Lenoir et al., 1994, Ring et al., 1997, Muhongo et al., 2002) and the Usagaran Belt contains a component of reworked Archean crustal fragments (Maboko and Nakamura, 1996, Möller et al., 1998, Maboko, 2000).

The KB, located to the west of the Tanzanian Craton (Figure 1), is made up of greenschist-to-amphibolite facies metasedimentary rocks intruded by numerous granitoids, and it records a magmatic intracratonic bimodal event at ~1375 Ma (Tack et al., 2010, Fernandez-Alonso et al., 2012). The Irumide Belt, located mainly in Zambia and Malawi, comprises a mix of gneisses and granite gneisses, plus a sequence of quartzite and pelite (De Waele and Mapani, 2002), and has deformation and metamorphism dated between 1100 and 950 Ma, with peak metamorphism at 1050-1000 Ma (Daly, 2007). In northern and central Mozambique, the Irumide Belt contains large volumes of orthogneiss emplaced between 1062 and 946 Ma, granulite-facies metamorphic rocks of ~953 Ma (Bingen et al., 2009, Sommer and Kröner, 2013).

Based on the geological background given above and in agreement with Roberts et al. (2012), the expected ages of the detrital zircon grains can be related to the following provenances: (i) 250 Ma and ~160 Ma: alkaline volcanics (associated with the East African Rift System, Roberts et al., 2012, and references therein), (ii) 650 Ma - 450 Ma: Mozambique Belt, late Pan-African event, (iii) 800 Ma - 650 Ma: Mozambique Belt, early Pan-African event, (iv) 1100 – 1000 Ma: Irumide Belt, (v) 1500 Ma - 1300 Ma: Kibaran Belt, (vi) 2100 Ma - 1800 Ma: UUB, and (vii) >2400Ma: Tanzanian Archean Craton.

### **The evolution of the Mandawa Basin and its sediment provenance**

The Mandawa Basin (Figure 2) of coastal southern Tanzania is one of many coastal rift basins located along the coast of East Africa that developed in response to the break-up of Gondwana during the early Mesozoic Era (Kent et al., 1971, Geiger et al., 2004, Schandelmeier et al., 2004, Nicholas et al. 2007, Hudson, 2010, Hudson & Nicholas 2015). Mesozoic sedimentation in the Mandawa Basin is largely controlled by variations in sea-level, with coarser-grained material being deposited in the central areas during times of

eustatic lowstand. The Mandawa Basin also experienced fully evaporitic conditions during the earlier stages of sedimentation (i.e. during the early Jurassic, or possibly Triassic periods). A period of tectonic stability lasted from the Late Cretaceous to Early Oligocene epochs and a passive margin developed along the coastal zone of the Mandawa Basin, where thick clay-prone successions defined as the Kilwa Group accumulated (Pearson et al., 2004, 2006, Nicholas et al., 2006, Berrocso et al., 2010, 2012, 2015).

Petrographic and conventional heavy mineral analyses have been performed by Nerbråten (2014) on selected Mesozoic and Cenozoic sandstones in the Mandawa Basin. Nerbråten (*op. cit.*) observes: (i) apatite ± garnet ± titanite in (?)Triassic/Jurassic alluvial sandstones, (ii) an ultrastable-rich HM assemblage in Late Jurassic coastal and tidal sandstones and in few Cretaceous deltaic sandstones, (iii) apatite ± garnet ± titanite ± zircon ± tourmaline in Cretaceous marine sandstones. In the onshore basin, the Cretaceous changes in the HM assemblage is attributed to either a change in sediment provenance within the Mandawa Basin and/or the preservation of less stable HM in the younger sediments.

A more recent study from Fossum et al. (2018) subdivided the analysed sandstones (Jurassic to Paleogene) in 4 groups according to characteristic heavy mineral types: 1) Garnet dominated (occurring regularly from the Middle Jurassic to the Eocene), (2) Calcic amphibole dominated (occurs in association with garnet, titanite, apatite and epidote, with minor kyanite and staurolite), (3) Zircon dominated (Upper Jurassic and Lower Cretaceous samples, and (4) Epidote dominated (Middle Eocene – Oligocene samples) sandstone associated with non-opaque heavy mineral species such as garnet, titanite, apatite, zircon and tourmaline. The integration of heavy mineral data with additional datasets derived from garnet and amphibole geochemistry, and detrital zircon geochronology were interpreted by the authors as reflecting a sediment supply sourced from several uplifted basement terranes and/or Karoo formations and conclude that the transportation system drained more or less the same terranes through most of Middle Jurassic to Eocene.

### **Sampling and methods**

15 samples have been collected from the northern and central portion of the Mandawa Basin (Figure 2) and span the Middle Jurassic (2 samples), Late Jurassic (4 samples) and Early Cretaceous (9 samples). In this paper, the samples are not assigned to specific formations, but are grouped by the broad ages of the sediment they occur within. Samples have been disaggregated and processed for heavy mineral separation (2.90 Na-polytungstate,

centrifuged and recovered by nitrogen freezing) and subsequent heavy mineral (optical, Raman and QEMSCAN for automated phase mapping) and grain varietal (garnet end-members and detrital zircon U-Pb dating) analyses.

### *Optical Heavy mineral analysis*

More than 200 transparent heavy minerals of detrital origin were optically identified in each sample using a polarizing microscope and counted applying the area method on fourteen of them (Galehouse, 1971, Mange and Maurer, 1992), while the point-count method has only been used on one sample (sample id: MDW - 164). Other transparent grains of suspected authigenic or spurious origin, including Ti aggregates, commonly resulted too numerous to count. Uncertainty during grain classification was eliminated by using Raman spectroscopy, which was also applied to identify anatase in crystals or Ti-aggregates.

### *Raman analysis*

Raman spectroscopy is used with the purpose of reducing the uncertainty in classifying the smallest grains for which optical properties are difficult to be observed. Spectra acquisition was obtained using an inVia Renishaw spectrometer equipped with a 532nm green laser using both 50x and 20x objectives. Spectra were collected after 20 cycles of 1 second acquisition in the spectral range 149-1900  $\text{cm}^{-1}$ . Grains were individually selected for analysis with time and focus being set by experienced operator. Further details on the collection of Raman spectra are available in Andò and Garzanti (2013). The spectrum of the bonding resin (Canada balsam) – the intense peaks of which may interfere with the diagnostic peaks of heavy minerals – was subtracted from collected spectra and the obtained Raman spectrum interpreted by comparison with literature data, public (e.g., RRUFF: <http://rruff.info>) and private (Laboratory of Provenance Analysis of Milano-Bicocca, Andò et al., 2011) mineralogical database. Raman spectroscopy was also applied to determine garnet types and end-members composition. Raman spectroscopy has been preferred to traditional microprobe analysis for a number of reasons. First, silt material is extremely fine. Handpicking 100 grains for microprobe analysis would be extremely difficult and potentially introduce biases related to selective choice of garnet crystals which are easier to identify because of coarser size or specific colours facilitating their identification. Secondly, mount polishing for microprobe sample preparation would easily determine a substantial loss of grains, hence reducing the number of analysed crystals and consequent statistical robustness of the dataset and interpretation. Garnet end-members were

recalculated following the approach of Bersani *et al.* (2009). The 6 main peaks characteristic of garnet types have been evaluated for each spectrum. Peak positions have been extracted (in  $\text{cm}^{-1}$  with an error of  $\pm 0.3 \text{ cm}^{-1}$ ) and processed after the fitting of a Gaussian-Lorentzian polynomial curve. The MIRAGEM algorithm (Bersani *et al.* 2009) was applied to assign the correspondent end-member to each grain— according to Mange and Morton 2007 - after obtaining the molar percentages for each garnet. In a few cases, uncertain intensity of diagnostic peaks related - for instance - to mineral orientation could cause a slight overestimation of a certain component (e.g. a pyrope with unusually high grossular component).

### *QEMSCAN analysis*

QEMSCAN (“Quantitative Evaluation of Minerals by SCANning electron microscopy”) is a scanning electron microscope equipped with an Energy Dispersive X-ray Spectra (EDS) detector. It produces detailed maps of the chemical composition of polished rock and mineral surfaces (Sutherland and Gottlieb, 1991, Allen *et al.*, 2012). These maps can be augmented with isotopic data by pairing the QEMSCAN instrument with a Laser Ablation Inductively Coupled Plasma Mass Spectrometer (LAICPMS). The resulting QEMSCAN+LAICPMS instrument suite greatly increases the throughput of igneous, metamorphic and detrital geochronology by reducing or entirely removing the need for mineral separation (Vermeesch *et al.*, 2017). In the context of sedimentary provenance analysis, QEMSCAN+LAICPMS does not only increase sample throughput, but also reduces selection bias as well (Vermeesch *et al.*, 2017, Garzanti *et al.*, 2018). In the present study, we have tasked the QEMSCAN to locate all zircon grains in a heavy mineral separate. The centre points of a representative number of these grains were then dated by the U-Pb method without further manual intervention..

### *Detrital zircon U/Pb geochronology*

The QEMSCAN “automated phase mapping” approach described in the previous section yielded >60 zircon grains for 11 out of our 15 samples, ensuring with 95% confidence that no fraction greater than 8.5% of the underlying population was missed (Vermeesch, 2004). Two samples yielded 46 and 39 zircons, respectively, thus incurring a 5% risk of missing at least one 12% or 10% fraction, respectively. The remaining two samples did not yield sufficient zircon to constrain a U-Pb age spectrum.

Zircon age measurements followed Jackson *et al.* (2004), and were performed using a New-Wave NWR193 excimer laser connected to an Agilent 7700x quadrupole ICPMS. Repeated measurements of external zircon standard Plešovice (TIMS reference age 337.13

$\pm 0.37$  Ma, Sláma et al., 2008) are used to correct for instrumental mass bias and depth-dependent inter-element fractionation of Pb, Th and U. Typical ablation parameters were 20  $\mu\text{m}$  spot size, 11 Hz repetition rate and an energy fluence of 2.2 J/cm<sup>2</sup>. Data reduction used Glitter 4.4 (Griffin et al., 2008) and age calculations followed Ludwig (1998, 2008). The calculated <sup>206</sup>Pb/<sup>238</sup>U age was used for grains younger than 1100 Ma, and the <sup>207</sup>Pb/<sup>206</sup>Pb age for older grains. Grains with a complex growth history or disturbed isotopic ratios, with > +5/-15% discordance, were rejected.

### *Statistical integration of the dataset*

Heavy mineral compositions from all datasets were analysed by principal component analysis (PCA) using Aitchison (1986)'s centred log-ratio (*clr*) transformation. The results of this analysis are represented as biplots. These consist of two superimposed 'maps' representing the samples and the variables (minerals). See Tolosana-Delgado et al. (2005) and Caracciolo et al. (2012) for further details about further details about the theoretical background and interpretation of biplots.

In addition to these *compositional* data, our dataset also comprises a number of *distributional* datasets (Vermeesch et al., 2016), including zircon U-Pb data and the single grain garnet compositions. These data are analysed by multidimensional scaling (MDS), an ordination technique that is closely related to PCA (Vermeesch, 2013). Given a table of pairwise 'dissimilarities' between 'objects', MDS produces a 'map' in which similar objects plot close together and dissimilar one plot far apart. In the context of this study, the 'objects' are samples and the 'dissimilarities' are given by the Kolmogorov-Smirnov statistic (Vermeesch, 2018).

Our study involves one compositional dataset and five distributional datasets. Individually analysing these data by PCA/MDS yields six pieces of graphical output. Jointly analysing this entire 'big' dataset is a non-trivial exercise that requires further statistical simplification. In this study, we will do so by means of three-way MDS (Vermeesch and Garzanti, 2015, Vermeesch et al., 2016). In contrast with conventional MDS, but similar to PCA, this technique produces not one but two pieces of graphical output.

The 'group configuration' displays the samples and represents a 'consensus' view obtained by jointly considering all the provenance proxies. In addition to this map, 3-way MDS produces a second scatter plot of the provenance proxies. This plot displays the 'weights' that each of the provenance proxies attach to the horizontal and vertical axis of the group configuration. The combination of the group configuration and the weights serves a similar purpose as the biplot discussed in the context of PCA.

## Results

### Heavy Mineral Analysis

The general heavy mineral content in analysed siltstone samples is rather low as demonstrated by correspondent values of the heavy mineral percentage, varying between 0.2% and 2.3% of separated material. A minimum of 200 transparent heavy minerals have been counted for each sample and classified according to both textural properties and degree of corrosion according to the catalogue included in Andò et al. (2012). Analytical results are shown in Table 1. The heavy minerals encountered during optical point count are (Table 1, Figure 3a): apatite (0-81%), zircon (4-62%), garnet (0-55%), tourmaline (6-40%, both dravite and schörl), titanite (0-21%), rutile (3-19%), epidote (0-14%), and lower amounts of staurolite (up to 5%), monazite (up to 2%), Cr-spinel (observed in only two samples) and kyanite (one sample). Other heavy minerals (e.g. anatase, biotite, carbonates, chlorite, and barite), rare light minerals, and rock fragments, although recognised, have been excluded from Table 1.

Jurassic samples are mainly dominated by apatite and ultrastable minerals (Ap% + ZTR = 97%). The sum of garnet, staurolite and kyanite is >50% in two samples only. The heavy mineral assemblage of Cretaceous samples of the central Mandawa basin is dominated by ultrastable minerals (zircon, tourmaline, rutile, ZTR $\geq$ 90%). The percentage of rounded heavy minerals is  $\leq$ 6%, and the one of subrounded grains is 9-34% with the highest concentration of rounded and sub-rounded grains observed in Early Cretaceous samples of the Southern Mandawa Basin. Between 15% and 56% of the observed heavy minerals are corroded (**Table 1**). The amount of rounded and subrounded heavy minerals is proportional with the abundance of ultrastable minerals, the percentage of corroded heavy minerals is inversely proportional with both apatite abundance and ZTR value (**Table 1**). The following mineralogical associations are highlighted by the compositional biplot (Figure 3b): apatite, garnet and the ultrastable ZTR group.

### Garnet typing

A total of 1015 garnet grains have been measured and processed for assignment to correspondent end-members (Figure 4a-d). Garnet types and field for provenance are those included in Mange and Morton (2007). Nine out of 15 samples hosted enough garnet grains to obtain statistically representative data for which 100 grains per sample were analysed. 2 samples (MDW-76 and MDW-318) were extremely poor in garnet, and only 4 and 11 grains respectively have been analysed. The 4 remaining samples delivered > 40 garnet for

analysis and end-member recalculation. Less than 1% of analysed garnets provided uncertain compositions including an unusually high pyrope and grossular component (Fig. 4a). According to Mange and Morton (2007) the large majority of garnet end-members consist of (Figure 4a) A (high-grade granulite facies metasediments) and Ci+Cii (high-grade metabasic and ultramafic rocks) types representing together more than 70% of analysed grains. Bi (granitoid and intermediate acid igneous rocks) and Bii (amphibolite facies metasediments) types vary in concentration between 20% and 30%, except in sample MDW-302 where they reach 58%. Other types occur in low concentrations and vary between 0% and 8%.

### **Detrital zircon U/Pb geochronology**

Jurassic samples contain abundant zircon grains displaying dominant age populations of 650-450 Ma, 650-800 Ma, and 1100-800 Ma and subordinate grain populations dated <300 Ma and 2100-1800 Ma (Figure 5a-b). Detrital zircons with ages 1500-1300 Ma and >2400 Ma have been also detected but in lower amounts and not in all samples. Sample MDW-294 (Southern Mandawa Basin) displays higher proportions of grains with ages of <300 Ma and 2100-1800 Ma than observed in other Middle Jurassic samples. Sample MDW-318 only shows detrital zircons populations of 650-450 Ma, 650-800 Ma, and 1100-800 Ma, however, the amount of detrital zircons identified and analysed for this sample is extremely low (n=16) and would therefore represent the most dominant set of populations only.

Cretaceous samples contain higher amounts of detrital zircon dated 650-450 Ma (Figure 5a-b). Three samples (MDW-813, MDW-32, and MDW-8\_39) also show abundant <300 Ma zircon grains, though the remaining samples show abundant 2100-1800 Ma zircon grains. Detrital zircon grains dated 1100-800 Ma are also common in most of the samples, whereas zircons dated 650-800 Ma are scarce. Zircon of >2400 Ma are low although significantly higher than in Jurassic samples (Fig. 5b).

Four Cretaceous samples contain abundant 650-450 Ma, 1100-800 Ma, 2100-800 Ma zircon ages, three samples (MDW-32, MDW-112, and MDW-220) also contain abundant <300 Ma and 650-800 Ma zircon ages. Moreover, the amount of >2400 Ma detrital zircon observed in Cretaceous samples is larger than those found in Jurassic samples (Fig. 5b).

## Discussion

### Compositional signatures and statistical data processing

#### *Heavy mineral assemblages*

Heavy mineral assemblages of fine-grained sediments of the Jurassic-Cretaceous Mandawa basin do not provide relevant information highlighting changes in provenance and/or modification to drainages between the Jurassic and Cretaceous (Fig. 3a). However, multivariate statistical data processing provides a better picture describing mineral associations and their variations in relation to sediment average composition. Three groups of variables consisting of garnet, apatite and ultrastable association of zircon, tourmaline and rutile (ZTR) are confidently established (Fig. 3b). The length of the links for garnet and apatite indicates much higher variability compared to ZTR which clearly represent most of the heavy mineral assemblage in each of the analysed samples. The geometrical relationships between these groups of variables suggest three distinct sources of sediments, with ZTR being representative of older sedimentary rocks. Apatite is likely related to acid igneous rock which are included in all of the terranes evaluated as potential source rocks of sediments. Point count data for textural typing of heavy minerals strengthen the idea of a polycyclic sedimentation and provide evidence suggesting depletion in heavy mineral species due to weathering/diagenetic processes. In fact, corroded grains increase proportionally to the decrease of ZTR minerals. If titanite is considered, apatite displays a higher association with ZTR suggesting that at least part of the latter may be linked to apatite, reflecting provenance from granitoid rocks (Figure 3b). Cretaceous samples have higher garnet and titanite compared to the Jurassic ones which are enriched in ZTR minerals. Such data are in agreement with previous studies (e.g. Nerbråten, 2014), especially regarding the ZTR, apatite, garnet and titanite detrital phases. Differences in amounts (e.g. titanite) are attributable to implicit differences in grain-size and consequent sediment fractionation.

#### *Single-grain compositional analysis*

Compositional signatures for garnet end-members (Figure 4) reflect erosion of dominantly high-grade granulite metasediments (Type A of Mange and Morton, 2007), low-moderate grade metasediments, granite and intermediate-acidic gneisses and amphibolite facies (Type Bi and Bii of Mange and Morton, 2007) with A, Bi and Bii types being more abundant in Jurassic samples while Ci and Cii in Cretaceous samples. The latter indicates

increasing sediment supply from metamafic lithologies through time. Although in different proportions, garnet types are in agreement to those reported in Fossum et al. (2018). Such differences can either be attributed grain-size (cfr. Krippner et al. 2016) or broader sediment routing system for silty sediments. The multi-dimensional scaling of almandine (Figure 4b) in particular show clear differences in terms of distribution and occurrence of Bi-Bii garnet types during Jurassic and Cretaceous sedimentation. However, changes in the proportion of garnet types through time are highlighted by the group configuration map including obtained from the 3-ways multidimensional scaling (Figure 4c). As for almandine, Jurassic and Cretaceous samples cluster in two different regions suggesting a different assemblage of garnet types and possibly the modification of the drainages transporting sediments into the Mandawa basin. The source weight for the 3-ways MDS display a configuration in which pyrope attaches equal weights to the X- and Y-dimension. However, the fact that the Cretaceous samples plot to the left of the Jurassic samples indicates that their grossular and almandine distributions are different. On the other hand, the fact that Cretaceous samples plot above the Jurassic samples indicates that their spessartine and andradite distributions are different with pyrope distributions affecting both dimensions equally. In terms of sediment provenance, both the MDS and 3-ways MDS provide additional elements indicating that to the increase of garnet and apatite correspond an increase of Ci and Cii types garnet and that, when all garnet types are considered, dissimilarities between Jurassic and Cretaceous samples consist in the different association and distribution of grossular-almandine and spessartine-andradite respectively.

KDE detrital zircon age distributions (Figure 5b) alone is already sufficient to visually estimate the differences between Jurassic and Cretaceous samples. The former include zircon displaying ages of mostly 650-450 Ma, 650-800 Ma, and 1100-800 Ma, corresponding to those from (i) the last Pan-African metamorphic terranes of the Mozambique Belt, (ii) the igneous emplacement event in the southern Mozambique Belt (early Pan-African event) and the Irumide Belt respectively. < 300 Ma ages are difficult to interpret and may be partly associated to the initiation of the Gondwana rifting event. Cretaceous samples have a different age distribution, especially in regard to the abundance of grains from the IB and UUB. Furthermore, they contain significantly higher amounts of Neoproterozoic zircon attributable to the Tanzanian Craton. The MDS (Figure 5c) enhances the difference between samples as they are strongly age-clustered in two groups with only one Cretaceous sample outlying and grouping with Jurassic samples.

### *Interpretation of paleo-drainages and sediment dispersal pathways*

Compositional signatures of Jurassic samples suggest a mixed provenance including recycling of older sedimentary successions and erosion of mostly felsic rocks. Indications from detrital zircon geochronology allow to confidently identify the Early- and Late Pan-African (gneisses-gneissic granite + quartzites and pelites – 1100-950 Ma, De Waele and Mapani, 2002) orogeny terranes of the MB and the IB as the main sources, with increasing sediment from the latter being eroded and transported during the Upper Jurassic – Cretaceous boundary. Contributions from the UUB are negligible at this time. Garnet end-members also vary, older samples being richer in A-type garnet derived from high-grade granulite metasediments and those from the Upper Jurassic being enriched in Bi- and Bii types derived from granite and amphibolite facies metasediments (Figures 4 and 6). Detrital zircon populations from Cretaceous samples document a significant broadening of the drainage system further extending into the IB and reaching as far as the granitoids and granitoid gneisses of the UUB (2000-1800 Ma magmatic ages, e.g. Collins et al., 2004) and those of the Tanzanian Archean Craton (>2500 Ma). Garnet compositional signatures of Cretaceous samples also indicate the broadening of paleodrainages which is represented by the marked increase in the pyrope component of detrital garnets (Figures 4 and 6). High-pressure rocks in eclogite-facies of the UUB and the metamafic rocks of UUB and the Archean Craton are the most likely source of Ci-Cii type detrital garnet during Cretaceous (Möller et al., 1995). The higher pyrope component suggests increasing erosion of eclogite terranes from the Jurassic to the Cretaceous. According to detrital zircon signatures, these terranes are identified in the eclogite of the Usagran and Ubendian belts (cfr. Boniface & Schenk). Although in small amounts, grossular (common in skarn and carbonatite) is only found in Cretaceous samples and, according to the occurrence in the region, is attributed to the Neoproterozoic Upper Ruvubu Alkaline Plutonic Complex (URAPC, Midende et al., 2014 and references therein) where carbonatite rocks are found in the Matongo Massif. The link to the URAPC is further strengthened by the 750 Ma age, a peak which increases in the detrital U-Pb age distribution included in this study (Figure 5).

### **3-way MDS**

The source weight for the 3-ways MDS including garnet, detrital zircon (DZ) and heavy mineral database display a configuration in which DZ and garnet weights determine the difference between Jurassic and Cretaceous samples (Figure 7). However, the fact that the Cretaceous samples plot to the left of the Jurassic samples indicates that their heavy mineral distribution is also different. Heavy mineral data, in fact, indicate increasing amounts of

garnet and titanite through time. On the other hand, source weights variations along the Y axis highlight the difference in DZ ages and garnet types between Jurassic and Cretaceous samples due to (i) increasing contribution from older terranes (UUB and Tanzanian Archean Craton) through time and (ii) garnet types changing in composition from dominantly A-Bi-Bii types to mostly A-Ci-Cii types. Compositional signatures included in this study are the same of those of Fossum et al. 2018. However, proportions between U-Pb age distribution and garnet end-members are different and lead to different conclusions. While Fossum et al. (2018) propose an unchanged sediment routing system between the Jurassic and the Eocene, our dataset support a broadening of the drainage system in the Cretaceous that increasingly extended as far as the Archean Craton and the Usagran-Ubendian and Kiraban-Urumide belts. Such differences are not necessarily related to data quality and/or interpretation but, more probably, to grain-size and hydraulic sorting controlled compositional features for heavy minerals, zircon and garnet.

## CONCLUSIONS

The analytical workflow and the processing of compositional data proposed in this paper constitute an example of how provenance of fine-grained sediments (silt) can be determined by using the same analytical routine applied - for the same scope - to sand and sandstone. In order to maximise the chances for successful analyses it is necessary to (i) perform high quality heavy mineral separation (using centrifuge and liquid nitrogen for separation and recovery respectively), (ii) double-check minerals of uncertain origin with the help of suitable instruments (iii) having access to Raman spectroscopy for discrimination of polymorphs and mineral typing (e.g. garnet, zircon etc.), (iv) use the automated phase mapping tool to get as much as datable grains avoiding biases introduced during grain handpicking.

The analytical workflow described above has been successful in recognising provenance changes and drainage modifications between Middle-Late Jurassic and Early Cretaceous Periods of the Mandawa Basin. Compositional signatures from heavy minerals are in agreement to those available in the literature and consist of dominant ZTR-apatite assemblage in Jurassic samples and increasing garnet and titanite during the Cretaceous. More relevant provenance signatures are provided by Raman garnet-end member analysis and detrital zircon U-Pb dating. Detrital garnet and zircon grains in Jurassic samples reflect contributions from mostly high-grade granulite and amphibolite facies metasediments and granitoid lithologies belonging to the terranes of the early- and late Pan-African Mozambique Belt and those of the Irumide Belt. Cretaceous samples record modifications and widening of

the drainage system extending as far as the granitoids and granitoid gneisses and the high-pressure rocks in eclogite-facies and the metamafic rocks of the Usagran-Ubendian Belt and Tanzanian Archean Craton.

#### ACKNOWLEDGEMENTS:

Dr. Chris Nicholas, Trinity College Dublin, is acknowledged for supplying the material for this paper. We thank Dr. James Utley and Dr. Andy Morton for the constructive criticism that contributed to the general improvement of the final version of this manuscript. Luca Caracciolo is indebted to Chemostrat Ltd., Sandtrak (Provenance Unit) and all the Employees for the time and experience acquired during the two years spent together and also acknowledge for allowing the publication of this manuscript.

#### REFERENCES

Aagard, P. 1974. Rare earth elements adsorption on clay minerals. *Bulletin du Groupe français des Argilles*, **26-2**, 193-199.

Alphin, A.C. & Macquacker, J.H.S. 2011. Mudstone diversity: Origin and implication of source, seal, and reservoir properties in petroleum systems. *AAPG Bulletin*, **95**, 2031-2059.

Andò, S., Garzanti, E., & Vignola, P. 2011. Raman counting A new method to determine provenance of silt. *Rendiconti Lincei. Scienze Fisiche e Naturali*, **22**, 327-347.

Andò, S., Garzanti, E., Padoan, M. & Limonta, M. 2012. Corrosion of heavy minerals during weathering and diagenesis: A catalog for optical analysis. *Sedimentary Geology*, **280**, 165-178.

Andò, S. & Garzanti, E. 2013. Raman spectroscopy in heavy-mineral studies. *Geological Society, London, Special Publications*, **386 (1)**, 395-412.

Armitage, P.J., Worden, R.H., Faulkner, D.R., Aplin, A.C., Butcher, A.R. & Iliffe, J. 2010. Diagenetic and sedimentary controls on porosity in Lower Carboniferous fine-grained lithologies, Krechba field, Algeria: A petrological study of a caprock to a carbon capture site. *Marine and Petroleum Geology*, **27**, 1395-1410.

Basu, A., Bickford, M. E. & Deasy, R. 2016. Inferring tectonic provenance of siliciclastic rocks from their chemical compositions: A dissent. In: Caracciolo, L., Garzanti, E., von Eynatten, H., Weltje, G.J. (eds) *Sediment generation and provenance: processes and pathways. Journal of Sedimentary Geology*, **336**, 26-35.

- Bersani, D., Andò, S., Vignola, P., Moltifiori, G., Marino, I.G., Lottici, P.P., & Diella, V. 2009. Micro-Raman spectroscopy as a routine tool for garnet analysis. *Spectrochimica Acta*, **73**, 484-491.
- Bingen, B., Jacobs, J., Viola, G., Henderson, I.H.C., Skår, Ø., Boyd, R., Thomas, R.J., Solli, A., Key, R.M. & Daudi, E.X.F. 2009. Geochronology of the Precambrian crust in the Mozambique Belt of NE Mozambique, and implications for Gondwana assembly. *Precambrian Research*, **170**, 231-255.
- Bloch, J. & Hutcheon, I.E. 1992. Shale diagenesis: a case study from the Albian Harmon Member (Peace river Formation), Western Canada. *Clays and Clay Minerals*, **40-6**, 682-699.
- Boniface, L. & Schenk, V. 2012. Neoproterozoic eclogites in the Paleoproterozoic Ubendian Belt of Tanzania: Evidence for a Pan-African suture between the Bangweulu Block and the Tanzania Craton. *Precambrian Research*. **208-211**, 72-89.
- Caracciolo, L., Von Eynatten, H., Tolosana-Delgado, R., Critelli, S., Manetti, P. & Marchev, P. 2012. Petrological, geochemical, and statistical analysis of Eocene-Oligocene sandstones of the western Thrace basin, Greece and Bulgaria. *Journal of Sedimentary Research*, **82**, 482–498.
- Caracciolo, L., Critelli, S., Cavazza, W., Meinhold, H., von Eynatten, H. & Manetti, P. 2015. The Rhodope Zone as a primary sediment source of the southern Thrace basin (NE Greece and NW Turkey): evidence from detrital heavy minerals and implications for central-eastern Mediterranean palaeogeography. *International Journal of Earth Sciences*, **104(3)**, 815-832.
- Caracciolo, L., Stone, T. & Barbarano, M. 2015. Quantitative Provenance Analysis of Heavy Minerals through Automated Raman Spectroscopy as a New Tool for the Petroleum Industry. *AAPG Middle East workshop: Siliciclastic reservoirs of the Middle East*, DOI10.13140/RG.2.1.3190.4802.
- Collins, A.S.S.M., Reddy, C., Buchan, A. & Mruma, A. 2004. Temporal constraints on Palaeoproterozoic eclogite formation and exhumation (Usagaran Orogen, Tanzania). *Earth and Planetary Science Letters*, **224**, 175 – 192.
- Cook, Y.A., Sanislav, I.V., Hammerli, J., Blenkinsop, T.G. & Dirks, P.H.G.M. 2016. A primitive mantle source for the Neoproterozoic mafic rocks from the Tanzania Craton. *Geoscience Frontiers*, **7**, 911-926.
- Daly, M.C. 2007. Geometry and evolution of the Mesoproterozoic Irumide Belt of Zambia. *Geological Society, London, Special Publications*, **272**, 223-230.

Dayal, A. M. 2017. Chapter 2: Deposition and Diagenesis. In: Exploration and Environmental and Economic Impacts (Ed. A.M. Dayal) .*Shale Gas*, 13–23.

De Waele B. & Mapani B. 2002. Geology and correlation of the central Irumide belt. *Journal of African Earth Sciences*, **35**, 385–397.

Dickinson, W.R. 1970. Interpreting detrital modes of graywacke and arkose. *Journal of Sedimentary Petrology*, **40**, 695–707.

Dypvik, H., O. Hankel, O. Nilsen, C. Kaaya, E & Kilembe. 2001. The Lithostratigraphy of the Karoo Supergroup in the Kilombero Rift Valley. Tanzania. *Journal of African Earth Sciences*, **2001**, **32(3)**, 451-70.

Fernandez-Alonso, M., Cutten, H., De Waele, B., Tack, L., Tahon, At, Baudet, D. & Barritt, S.D. 2012. The Mesoproterozoic Karagwe-Ankole Belt (formerly the NE Kibara Belt): The result of prolonged extensional intracratonic basin development punctuated by two short-lived far-field compressional events. *Precambrian Research*, **216-219**, 63-86.

Fossum, K., Morton, A., Dypvik, H. & Hudson, W. 2018. Integrated heavy mineral study of Jurassic to Paleogene sandstones in the Mandawa Basin, Tanzania: Sediment provenance and source-to-sink relations. *Journal of African Earth Sciences*, **150**, 546-565. Frysinger, G.R. & Thomas, H.C. 1960. Adsorption studies on clay minerals. VII Yttrium-Cesium and Cerium (III)-Cesium on montmorillonite. *Journal of Physical Chemistry*, **64**, 2, 224-228.

Fritz, H., Abdelsalam, M., Ali, K. A., Bingen, B., Collins, A. S., Fowler, A. R., Ghebreab, W., Hauzenberger, C. A., Johnson, P. R., Kusky, T. M., Macey, P., Muhongo, S., Stern, R. J. & Viola, G. 2013. Orogen styles in the East African Orogen: A review of the Neoproterozoic to Cambrian tectonic evolution, *Journal of South African Earth Sciences*, **86**, 65–106.

Frysinger, G. R. & Thomas, H.C. 1960. Adsorption studies on clay minerals. VII. yttrium-cesium and cerium (iii)-cesium on montmorillonite. *Physical Chemistry*, **64 (2)**, 224–228. DOI: 10.1021/j100831a010.

Garzanti, E., Doglioni, C., Vezzoli, G. & Andò, S. 2007. Orogenic Belts and Orogenic Sediment Provenance. *The Journal of Geology*, **115-3**, 315-334.

Garzanti, E., Andò, S., France-Lanord, C., Censi, P., Vignola, P., Galy, V. & Lupker, M. 2011. Mineralogical and chemical variability of fluvial sediments 2. Suspended-load silt

(Ganga-Brahmaputra, Bangladesh). *Earth and Planetary Science Letters*, **302(1)**, 107-120

Garzanti, E. & Resentini, A. (2016), Provenance control on chemical indices of weathering (Taiwan river sands). *Journal of Sedimentary Geology*, In: Sediment generation and provenance: processes and pathways, 336, 81-95.

Gasharova, B., Mihailova, B. & Konstantinov, L. 1997. Raman spectra of various types of tourmaline. *European Journal of Mineralogy*, **9(5)**, 935-940

Gazzi, P. 1966. Le Arenarie del Flysch Sopracretaceo dell'Appennino Modenese: Correlazioni con il Flysch di Monghidoro. *Mineralogica e Petrografica Acta*, **12**, 69–97.

Geele, C., De Wit, M., Booth, P., Schulz, H-M. & Horsfield, B. 2015. Palaeo-environment, diagenesis and characteristics of Permian black shales in the lower Karoo Supergroup flanking the cape fold belt near Jansenville, Eastern Cape, South Africa: implications for the shale gas potential of the Karoo basin. *South African Journal of Geology*, **118 (3)**, 249-274.

Geiger, M., Clark, D.N. & Mette, W. 2004. Reappraisal of the timing of the breakup of Gondwana based on sedimentological and seismic evidence from the Morondava Basin, Madagascar. *Journal of South African Earth Sciences*, **38**, 363–381.

Griffin, W.L., Powell, W.J., Pearson, N.J. & O'Reilly S.Y. 2008. GLITTER: data reduction software for laser ablation ICP-MS. In: *Sylvester, P. (Ed.), Mineralogical Association of Canada Short Course Series, Vancouver, B.C., 2008, 40*, 204–207. Appendix 2.

Hoang, L.H., Thi Minh Hien, N., Bai Chen, X., Van Minh, N. & Yang, I. 2011. Raman spectroscopic study of various types of tourmalines. *Journal of Raman Spectroscopy*, **42**, 1442-1446.

Hudson, W. E., 2010. The geological evolution of the petroleum prospective Mandawa Basin. Southern coastal Tanzania. Unpublished Ph.D. thesis. Trinity College Dublin.

Hudson, W.E. & Nicholas, C.J. 2014. The Pindiro Group (Triassic to Early Jurassic Mandawa Basin, southern coastal Tanzania): Definition, palaeoenvironment, and stratigraphy. *Journal of African Earth Sciences*, **92**, 55–67.

Ingersoll, R.V. 1990. Actualistic sandstone petrofacies: discriminating modern and ancient source rocks. *Geology*, **18**, 733-736.

Jackson, S. E., Pearson, N. J., Griffin, W. L. & Belousova, E. A. 2004. The application of

laser ablation-inductively coupled plasma-mass spectrometry to in situ U/Pb zircon geochronology, *Chemical Geology*, **211**, 47–69.

Jochum, K.P., Weis, U., Stoll, B., Kuzmin, D., Yang, Q.C., Raczek, I., Jacob, D.E., Stracke, A., Birbaum, K., Frick, D.A., Gunther, D. & Enzweiler, J. 2011. Determination of reference values for NIST SRM 610–617 glasses following ISO guidelines. *Geostandard and Geoanalytical Research*, **35**, 397-429.

Kabete, J., Groves, D.I., McNaughton, N.J., Mruma, A.H. 2008. A new tectonic subdivision of the Archean Craton of Tanzania and its significance to gold metallogeny. *Extended Abstract Volume, SEG-GSSA 2008*.

Kreuser, T., Wopfner, H., Kaaya, C. Z., Markwort, S., Semkiwa, P. M. & Aslanidis, P. 1990. Depositional evolution of Permo- Triassic Karoo Basins in Tanzania with reference to their economic potential. *Journal of African Earth Sciences*, **10 (1/2)**, 151-167.

Kröner A., Muhongo S., Hugner E. & Wingate M.T.D. 2003. Single-zircon geochronology and Nd isotopic systematics of proterozoic high-grade rocks from the Mozambique Belt of Southern Tanzania (Masasi area): Implications for Gondwana assembly. *Journal of the Geological Society, London*, **160**, 745-757.

Laughrey, C.D., Ruble, T.E., Lemmens, H., Kostelnik, J., Butcher, A.R., Walker, G., & Knowles, W. 2011. Black shale diagenesis: insights from integrated high-definition analyses of post-mature Marcellus Formation rocks, northeastern Pennsylvania. *Search and Discovery Article #110150*.

Layley, C.J.M., Selby, D., Condon, D.J., Horstwood, M.S.A., Millar, I., Crowley, Q. & Imber, J. 2013. Lithogeochemistry, geochronology and geodynamic setting of the Lupa Terrane, Tanzania: Implications for the extent of the Archean Tanzanian Craton. *Precambrian Research*, **231**, 174-193.

Lihou, J. C. & Mange-Rajetzky, M. A. 1996. Provenance of the Sardona Flysch, eastern Swiss Alps: examples of high-resolution heavy mineral analysis applied to an ultrastable assemblage. *Sedimentary Geology*, **105 (3-4)**, 141-157.

Ludwig, K.R. 1998. On the treatment of concordant uranium-lead ages. *Geochimica Et Cosmochimica Acta*, **62**, 665-676.

Ludwig, K.R. 2008. Isoplot/Ex 3.70. A Geochronological Toolkit for Microsoft Excel. *Berkely Special publication*, **4**, 76 pp.

Maboko, M.A.H. & Nakamura, E. 1996 Nd and Sr isotopic mapping of the Archæan-Proterozoic boundary in southeastern Tanzania using granites as probes for crustal growth. *Precambrian Research*, **77**, 105 - 115.

Maboko, M.A.H. 2000. Nd and Sr isotopic investigation of the Archean-Proterozoic boundary in north eastern Tanzania: constraints on the nature of Neoproterozoic tectonism in the Mozambique Belt. *Precambrian Research*, **102**, 87–98.

Mange, M.A. & Morton, A.C. 2007 Geochemistry of heavy minerals. *In: Heavy minerals in use: Developments in Sedimentology*, Mange, M.A., Wright, D.T. (Eds.), **58**, 345–391.

Maksimović Z., White, J.L. & Logar, M. 1981. Chromium-bearing dickite and chromium-bearing kaolinite from Teslić Yugoslavia. *Clays and Clay Minerals*, **29 (3)**, 213-218.

Mansur, A. 2008. Composition, age, and origin of the lower crust in northern Tanzania. *Master's Thesis, University of Maryland College-Park*. <http://hdl.handle.net/1903/8993>.

Midende, G., Boulvais, P., Tack, L., Melcher, F., Gerdes, A., Dewaele, S., Demaiffe, D. & Decrée, S. 2014. Petrography, geochemistry and U–Pb zircon age of the Matongo carbonatite Massif (Burundi): Implication for the Neoproterozoic geodynamic evolution of Central Africa. *Journal of African Earth Sciences*, **100**, 656-674.

Morris, N.J., Gardner, D. & Glemser, C. 2014. Upper Montney Geochemistry: Insights into Sedimentary Provenance. *GeoConvention 2014: Focus*, 4 pp.

Möller, A., Appel, P., Mezger, K. & Schenk, V. 1995. Evidence for a 2 Ga subduction zone: Eclogites in the Usagaran belt of Tanzania. *Geology*, **23(12)**, 1067-1070.

Möller, A., Mezger, K. & Schenk, V. 1998. Crustal age domains and the evolution of the continental crust in the Mozambique Belt of Tanzania: combined Sm–Nd, Rb–Sr and Pb–Pb isotopic evidence. *Journal of Petrology*, **39**, 749–783.

Muhongo, S., Tuisku, P., Mnali, S., Temu, E., Appel, P. & Stendal, H. 2002. High-pressure granulite-facies metagabbros in the Ubendian Belt of SW Tanzania: preliminary petrography and P–T estimates. Short communication. *Journal of South African Earth Sciences*, **34**, 279–285.

Nasdala, L., Smith, D.C., Kaindl, R. & Ziemann, M.A. 2004. Raman spectroscopy: Analytical perspectives in mineralogical research (Chapter 7). *MU Notes in Mineralogy*, **6**, 281–343.

Nerbråten, K. 2014. Petrology and Sedimentary Provenance of Mesozoic and Cenozoic Sequences in the Mandawa Basin. *Ph.D. Thesis* (<https://www.duo.uio.no/handle/10852/41482>),

Nesbitt, H. W. & Markovics, G. 1997. Weathering of granodioritic crust, long-term storage of elements in weathering profiles, and petrogenesis of silicate sediments. *Geochemica et Cosmochemica Acta*, **61 (8)**, 1653 – 1670.

Nicholas, C. J., Pearson, P. N., Bown, P. R., Dunkley-Jones, T., Huber, B. T., Karega, A., Lees, J. A., McMillan, I. K., O'Halloran, A., Singano, J. M. & Wade, B. S. 2006. Stratigraphy and sedimentology of the Upper Cretaceous to Paleogene Kilwa Group, southern coastal Tanzania. *Journal of African Earth Sciences*, **45**, 431 - 466.

Nicholas, C. J., Pearson, P. N., McMillan, I. K., Ditchfield, P. W. & Singano, J. M., 2007. Structural evolution of southern coastal Tanzania since the Jurassic. *Journal of African Earth Sciences*, **48**, 273 - 297.

Pearson, P.N., Nicholas, C.J., Singano, J.M., Bown, P.R., Coxall, H.K., van Dongen, B.E., Huber, B.T., Karega, A., Lees, J.A., Msaky, E., Pancost, R.D., Pearson, M. & Roberts, A.P. 2004. Paleogene and Cretaceous sediment cores from the Kilwa and Lindi areas of coastal Tanzania: Tanzania Drilling Project Sites 1–5. *Journal of African Earth Sciences*, **39**, 25–62.

Pearson, P.N., Nicholas, C.J., Singano, J.M., Bown, P.R., Coxall, H.K., van Dongen, B.E., Huber, B.T., Karega, A., Lees, J.A., MacLeod, K., McMillan, I.K., Pancost, R.D., Pearson, M. & Msaky, E. 2006. Further Paleogene and Cretaceous sediment cores from the Kilwa area of coastal Tanzania: Tanzania Drilling Project Sites 6–10. *Journal of African Earth Sciences*, **45**, 279–317.

Prince, C. M., Steele, D.D., Zelaya, R. & Devier, C. A. 2011. Shale Diagenesis and Permeability: Examples from the Barnett Shale and the Marcellus Formation. *Search and Discovery Article*, #50372.

Roberts, E.M., Stevens, N.J., O'Connor, P.M., Dirks, P.H.G.D.M., Gottfried, M.D., Clyde, W.C., Armstrong, R.A., Kemp, I.S. & Hemming, S. 2012. Initiation of the western branch of the East African Rift coeval with the eastern branch. *Nature Geoscience*, **5**, 289–294.

Ring, U., Kröner, A. & Toulkeridis, T. 1997. Palaeoproterozoic granulite-facies metamorphism and granitoid intrusions in the Ubendian-Usagaran Orogen of northern Malawi, east-central Africa. *Precambrian Research*, **85**, 27–51.

Salman, G. & Abdula, I. 1995. Development of the Mozambique and Ruvuma sedimentary basins, offshore Mozambique. *Sedimentary Geology*, **96**, 7–41.

Schandelmeier, H., Bremer, F. & Holl, H.G. 2004. Kinematic evolution of the Morondava rift basin of SW Madagascar—from wrench tectonics to normal extension. *Journal of African Earth Sciences*, **38(4)**, 321–330.

Skultéti, Á., T.M. Tóth, K. Fintor & F. Schubert. 2014. Deformation history reconstruction using single quartz grain Raman microspectroscopy data. *Journal of Raman Spectroscopy*, **45(4)**, 314–321.

Sláma, J., Košler, J., Condon, D.J., Crowley, J.L., Gerdes, A., Hanchar, J.M. & Whitehouse, M.J. 2008. Plešovice zircon—a new natural reference material for U–Pb and Hf isotopic microanalysis. *Chemical Geology*, **249**, 1–35.

Sommer, H., Kröner, A., Hauzenberger, C.H. & Muhongo, S. 2003. Metamorphic petrology and zircon geochronology of high-grade rocks from the central Mozambique belt of Tanzania. *Journal of Metamorphic Geology*, **21**, 915–934.

Sommer, H., Kröner, A., Muhongo, S. & Hauzenberger, C. 2005. SHRIMP zircon ages for post-Usagaran granitoid and rhyolitic rocks from the Paleoproterozoic terrain of south-western Tanzania. *South African Journal of Geology*, **108**, 247–256.

Sommer, H. & Kröner, A. 2013. Ultra-high temperature granulite-facies metamorphic rocks from the Mozambique belt of SW Tanzania. *Lithos*, **170–171**, 117–143.

Sutherland, D. & Gottlieb, P. 1991. Application of automated quantitative mineralogy in mineral processing. *Minerals Engineering*, **4(7–11)**, 753–762.

Syed, H.S. 1999. Comparison studies adsorption of thorium and uranium on pure clay minerals and local Malaysian soil sediments. *Journal of Radioanalytical and Nuclear Chemistry*, **241**, 11–14.

Tack, L., Wingate, M.T.D., De Waele, B., Meert, J., Belousova, E., Griffin, B., Tahona, A. & Fernandez-Alonso, M. 2010. The 1375 Ma “Kibaran event” in Central Africa: Prominent emplacement of bimodal magmatism under extensional regime. *Precambrian Research*, **180**, 63-84.

Taylor, S.R. & McLennan, S.M. 1985. The Continental Crust, Its composition and evolution, an examination of the geochemical record preserved in sedimentary rocks. *Blackwell, Oxford*. 312 p.

Tenczer, V., Hauzenberger, C. A., Fritz, H., Whitehouse, M. J., Mogessie, A., Wallbrecher, E., Muhongo, S. & Hoinkes, G. 2006. Anorthosites in the Eastern Granulites of Tanzania- New SIMS zircon U-Pb age data, petrography and geochemistry. *Precambrian Research*, **148**, 85–114.

Tolosana-Delgado, R., Otero, N., Pawlowsky-Glahn, V. & Soler, A. 2005. Latent compositional factors in the Llobregat river basin (Spain) hydrogeochemistry. *Mathematical Geology*, **37 (7)**, 681–702.

Tribouillard, N., Alego, T. J., Lyons, T., & Riboulleau, A. 2006. Trace metals as paleoredox and paleoproductivity proxies: an update. *Chemical Geology*, **232**, 12-32.

Valloni, R. & Maynard B.J. 1981. Detrital Modes of Recent Deep-Sea Sands and their Relation to Tectonic Setting: A First Approximation. *Sedimentology*, **31**, 353-364.

Vermeesch, P. & Garzanti, E. 2015. Making geological sense of ‘Big Data’ in sedimentary provenance analysis. *Chemical Geology*, **409**, 20–27.

Vermeesch, P., Resentini, A. & Garzanti, E. 2016. An R package for statistical provenance analysis. *Sedimentary Geology*, **336**, 14–25.

Vermeesch, P., Rittner, M., Petrou, E., Omma, J., Mattinson, C. & Garzanti, E. 2017. High Throughput Petrochronology and Sedimentary Provenance Analysis by Automated Phase Mapping and LAICPMS. *G<sup>3</sup> Geochemistry, Geophysics, Geosystems*, **18**, 4096–4109.

von Eynatten, H. & R. Gaupp. 1999. Provenance of Cretaceous synorogenic sandstones in the Eastern Alps: constraints from framework petrography, heavy minerals and mineral chemistry. *Sedimentary Geology*, **124**, 81-111.

von Eynatten, H. & Dunkl, I. 2012. Assessing the sediment factory: The role of single grain analysis. *Earth Science Reviews*, **115**, 97-120.

Zuffa, G.G. 1985. Optical analyses of arenites: influence of methodology on compositional results. in Zuffa, G.G., ed., *Provenance of Arenites: Dordrecht, D. Reidel, NATO ASI, Series 148*, 165–189.

## FIGURE CAPTIONS

Figure 1. Simplified geological map of central Tanzania. A. Metamorphic terranes and associated sedimentary basins. B. Geochronological map of terranes of Central Tanzania.

Figure 2. A. Simplified geological Map of the Mandawa Basin and sampling location. B. Stratigraphic sketch of the Mandawa Basin (modified after Hudson, 2011) showing the relative position of Cretaceous and Jurassic samples selected for this study.

Figure 3. Summary panel showing: A) Heavy mineral assemblages for Jurassic (MDW-294 to MDW 328) and Cretaceous (MDW-8\_39 to MDW-32) samples, B) Biplot showing the variability of most relevant heavy minerals (right side biplot includes titanite), C) Representative Raman spectra of heavy minerals from the Mesozoic Mandawa Basin.

Figure 4. Raman garnet typing and end-members recalculation. A) Garnet end-members including lithological fields for provenance (according to Mange and Morton, 2007), B) Multi-dimensional scaling (MDS) highlighting the difference in Almandine content between Jurassic and Cretaceous samples. C) 3-way multidimensional scaling showing different provenance features and sourcing lithologies between Jurassic and Cretaceous samples (see explanation in the text, D) Raman spectra of garnet types belonging to Pyralspites (spessartine, almandine and pyrope) and Grandites (grossular and andradite) groups.

Figure 5. Detrital zircon age distribution in silt samples of the Mesozoic Mandawa Basin. A) Summary probability density plot (PDP) of ages derived from U-Pb dating of 983 detrital zircon and their association to main metamorphic events and related terranes in Tanzania, B) Detailed view of age distributions for analysed samples highlighting the increasing contribution from the Irumide Belt, Ubendian-Usagran Belt and Archean Craton through time, C) Multi-dimensional scaling showing the marked difference in zircon age distribution between Jurassic and Cretaceous samples.

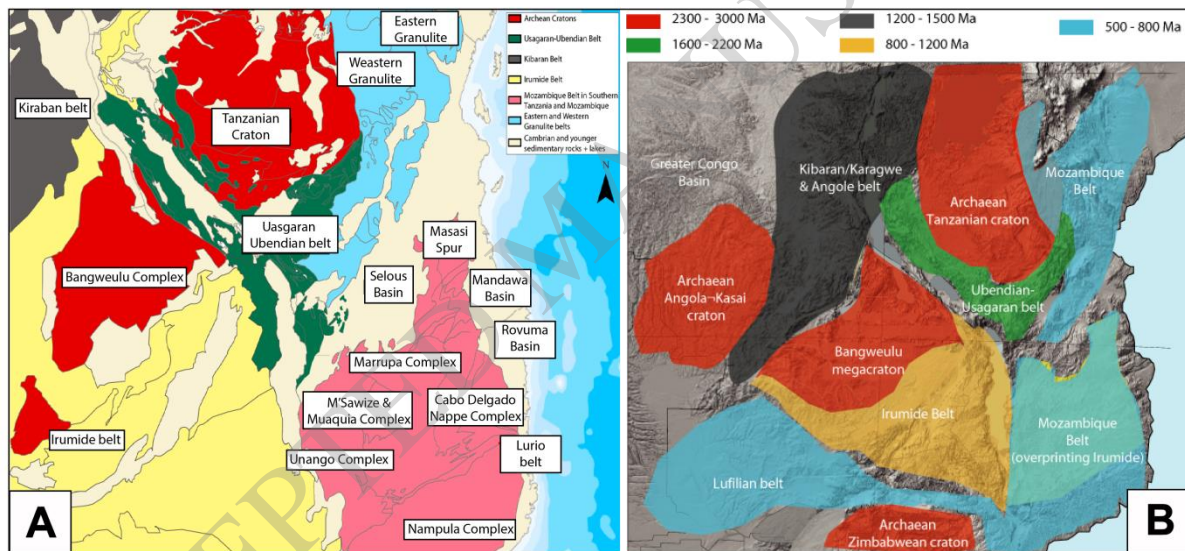
Figure 6. Compositional summary panel including datasets from detrital geochronology, garnet-end members and heavy minerals derived from both Raman-aided optical point count showing related compositional changes through time. A, Bi, Bii, Ci, Cii correspond to the lithological fields of provenance of Mange and Morton, 2007, HM= heavy minerals, Ap=apatite, Sch=schörl, Rt=rutile, Grt=garnet, Zr=zircon, Tu= Tourmaline.

Figure 7. 3-way multidimensional scaling basing on heavy mineral, garnet end-members and detrital zircon databases. The source weights box explains compositional variations: on the X axis, differences are related to heavy minerals assemblages, Y axis, differences consist of different detrital zircon age distribution and garnet end-members abundances between Jurassic and Cretaceous samples (cfr. explanation in the text).

ACCEPTED MANUSCRIPT

Table 1

Sample (Optical)	Age/Position	Zircon	Tourmaline	Rutile	Titanite	Apatite	Monzonite	Chromite	Epitaxial	Garnet	Staurolite	Kyanite	Thermometer	Zirconium	% R	% sR	% Corrod
MDW-294	Jurassic/North	1 8.5	10.9	7.6	3.3	33.2	0.0	0.0	0.0	26.5	0.0	0.0	3.7	4.7	30.1	36.7	
MDW-269	Jurassic/North	1 5.5	15.5	7.3	1.5	14.6	1.9	0.0	0.0	43.2	0.0	0.0	3.8	4.4	33.3	50.7	
MDW-300	Jurassic/North	1 8.0	16.1	3.4	0.0	39.5	0.5	0.0	0.0	22.4	0.0	0.0	3.8	4.4	32.2	40.7	
MDW-302	Jurassic/North	2 4.6	12.5	8.9	0.0	25.9	0.4	0.0	0.0	27.7	0.0	0.0	4.6	2.9	31.7	43.8	
MDW-318	Jurassic/South	4.0	6.0	6.0	0.0	80.6	0.0	0.0	0.0	3.5	0.0	0.0	1.6	2.5	14.7	24.9	
MDW-328	Jurassic/South	1 8.2	10.9	6.8	18.2	9.5	1.8	0.0	4.5	28.6	1.4	0.0	3.6	6.1	30.5	37.5	
MDW-220	Cretaceous/North	1 0.3	10.3	4.2	0.0	19.6	0.0	0.0	0.0	55.1	0.5	0.0	2.5	2.3	8.6	56.1	
MDW-76	Cretaceous/Central	3 6.3	40.3	3.4	0.0	0.0	0.5	0.5	0.0	3.0	5.5	5.5	9.0	5.5	21.9	22.9	
MDW-08_13A	Cretaceous/Central	1 3.5	17.4	5.8	0.0	34.8	0.0	0.5	0.0	28.0	0.0	0.0	3.7	3.4	34.3	44.7	
MDW-08_39A	Cretaceous/Central	1 9.7	16.1	6.0	0.0	34.4	0.0	0.0	0.0	23.4	0.5	0.0	4.2	3.0	30.5	28.9	
MDW-97	Cretaceous/Central	1 9.9	11.8	3.4	14.8	20.2	0.5	0.0	0.0	37.9	1.5	0.0	2.5	2.7	26.8	42.6	
MDW-112	Cretaceous/Central	1 0.0	9.1	3.3	21.1	3.8	0.0	0.0	13.9	37.8	0.0	0.0	2.3	4.1	22.2	36.8	
MDW-164	Cretaceous/South	8.0	6.5	5.0	0.0	27.0	0.5	0.0	0.0	52.0	1.0	0.0	2.0	3.0	24.0	36.8	
MDW-32	Cretaceous/South	1 3.3	19.4	0.4	1.9	28.9	0.0	0.0	5.5	24.6	0.9	0.0	4.3	2.4	24.9	28.9	



ACCEPTED MANUSCRIPT



